Notes

Contribution from the Research Laboratory of Engineering Materials, Tokyo Institute of Technology, 4259 Nagatsuta, Midori-ku, Yokohama 227, Japan

Raman Spectral Study of the Molten $ZnCl_2$–KCl System

Mitsuru Itoh,* Kazuo Sakai, and Tetsurō Nakamura

Received October 20, 1981

The structure of molten zinc chloride is of considerable interest because its physical properties indicate the occurrence of an extensive molecular association. Moreover, the molten $ZnCl_2$–ACl system (A = alkali metals) has been considered to be a low-temperature model of the silicate system SiO_2–BO (B = alkaline-earth metals) or the fluoride system BeF_2–AF (A = alkali metals) because of a similarity of polymeric nature[1,2] in the molten state. A polymeric structure for this system has been proposed on the basis of indirect studies, i.e., measurements of density,[3] ultrasonic velocity,[4] absorption of ultrasonic waves,[5] viscosity,[6] etc. The results suggest that a certain $(ZnCl_2)_n$ polymer in the molten pure $ZnCl_2$ is dissociated gradually on increasing temperature or on addition of excess chlorine ion. A recent report on X-ray radial distribution analysis by Triolo and Narten,[7] however, has proved that the molten $ZnCl_2$ consists of $ZnCl_4$ units. Raman spectral studies on the $ZnCl_2$–KCl system have been reported by Bues,[8] Bues and Brockner,[9] Moyer et al.,[10] and Ellis,[11] which proposed various complex ions shown in Table I.

In this report we investigated also the existence of several complex ions in the molten $ZnCl_2$–KCl system via the Raman spectra vs. temperature or concentration.

Experimental Section

The method for purification of $ZnCl_2$ is the same as previously reported.[12] Crude commercial reagent $ZnCl_2$ (99.9% purity), together with zinc metal (99.999% purity), was put into a quartz vessel for further chemical manipulation. The $ZnCl_2$ was dried under vacuum at 443 K for 1 day. After that, purified chlorine gas was passed over the sample heated at 443 K for 10 h. In the final purification, the sample was fused and chlorine gas was bubbled through the melt held at 700 K for 10 h, followed by bubbling of argon gas to remove the dissolved chlorine gas. After the sample was transferred into the side tube (Raman cell) of 1.6 cm diameter and 0.15 cm thickness, the whole system was held under vacuum. The sample was allowed to cool gradually to room temperature and then stored in the tube. The samples with intermediate concentrations were prepared from KCl, dried under vacuum at 473 K for 1 day, and the purified $ZnCl_2$ by means of the method mentioned above.

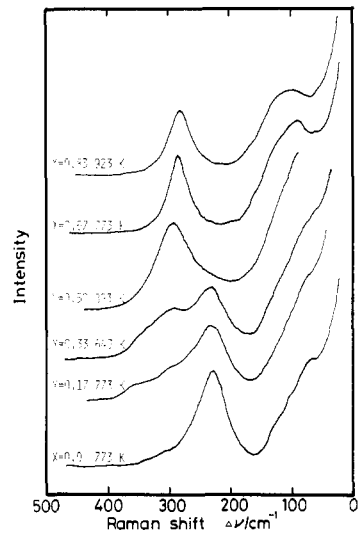

Figure 1. Concentration dependences of Raman spectra of the molten $ZnCl_2$–KCl system.

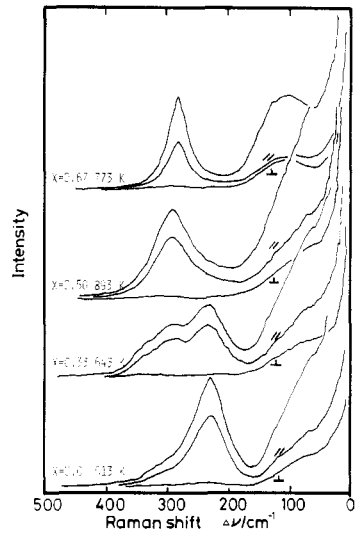

Figure 2. Polarized Raman spectra of molten $ZnCl_2$–KCl system: (∥) parallel polarization; (⊥) perpendicular polarization.

Raman spectra were recorded with a JEOL laser-Raman spectrophotometer (Model JRS 400D) equipped with 514.5-nm excitation radiation from an argon ion laser for the spectra of the chloride melts. The spectral resolution associated with slit width in the measurement of Raman spectra was narrower than 1.2 cm^{-1}. The temperature of the sample was measured with a chromel–alumel thermocouple outside the Raman cell. The accuracy of the temperature measurements of the sample was ±7 K, and a local temperature rise in the sample during the laser irradiation may be ignored for such a transparent molten salt system as the $ZnCl_2$–KCl system.

Results and Discussion

Figures 1 and 2 show the Raman spectra for several concentrations in the molten $ZnCl_2$–KCl system where some spectra were compared with the spectra observed by insertion of a polarizer. The spectra are characterized by the two intense and polarized bands located in the range from 200 to 300 cm^{-1} and the other broad and depolarized band in the range from

(1) Moynihan, C. T.; Canter, S. *J. Chem. Phys.* **1968**, *48*, 115.
(2) Canter, S.; Ward, W. T.; Moynihan, C. T. *J. Chem. Phys.* **1969**, *50*, 2874.
(3) Yokō, T.; Crescent, R.; Tsukagoshi, Y.; Ejima, T. *Nippon Kinzoku Gakkaishi* **1978**, *42*, 1179.
(4) Yokō, T.; Nakano, M.; Ejima, T. *Nippon Kinzoku Gakkaishi* **1980**, *44*, 508.
(5) Yokō, T.; Nakano, M.; Ejima, T. *Nippon Kinzoku Gakkaishi* **1980**, *44*, 516.
(6) Ejima, T.; Yokō, T.; Nakashima, K. *Nippon Kinzoku Gakkaishi* **1977**, *41*, 86.
(7) Triolo, R.; Narten, A. H. *J. Chem. Phys.* **1981**, *73*, 703.
(8) Bues, W. *Z. Anorg. Allg. Chem.* **1955**, *279*, 104.
(9) Bues, W.; Brockner, W. *Z. Phys. Chem. (Wiesbaden)* **1974**, *88*, 290.
(10) Moyer, J. L.; Evans, J. C.; Lo, G. Y-S. *J. Electrochem. Soc.* **1966**, *113*, 158.
(11) Ellis, R. B. *J. Electrochem. Soc.* **1966**, *113*, 485.
(12) Itoh, M.; Nakamura, T.; Sata, T., submitted for publication in *J. Electrochem. Soc.*

0020-1669/82/1321-3552$01.25/0

Table I. Literature Data on Raman Spectra for the Molten $ZnCl_2$–KCl System

ref	compn	Raman shift $\Delta\nu$, cm^{-1} [a]							
8	$ZnCl_2$		233	233			292		
	$2ZnCl_2 \cdot 1KCl$			233			292		
	$1ZnCl_2 \cdot 1KCl$	85					292		
	$1ZnCl_2 \cdot 2KCl$	92				280			
	$1ZnCl_2 \cdot 4KCl$	92				280			
	assignt			poly		$ZnCl_4^{2-}$	$ZnCl_3^-$		
10	$ZnCl_2$	75 w		226 s, p	250 w			305 w	306 w
	$4ZnCl_2 \cdot 1KCl$	80 w		226 s, p			288 w, p		349 w
	$2ZnCl_2 \cdot 1KCl$	75 w		226 s, p			290 w, p		344 w, p
	$1ZnCl_2 \cdot 1KCl$	80 w	125 w	218 vw			292 m, p		
	$2ZnCl_2 \cdot 3KCl$	70 w	120 w				294 s, p		
	$1ZnCl_2 \cdot 2KCl$	75 w	124 w				283 s, p		
	assignt	poly, b, def		poly, b	poly, b		poly, t	poly, t	poly, t
14	$ZnCl_2$			230	266			305	
	assignt			poly	$ZnCl_n^{2-n}$			$ZnCl_2$	
	$ZnCl_2$	80 w, d	90, w, d	227, s, p	270 w, p			310 w, p	350 vw
	$9ZnCl_2 \cdot 1KCl$	82 w, d	106 2, p	230 s, p	262 w, p			300 w, p	340 w, p
	$7ZnCl_2 \cdot 1KCl$		95 w, d	232 s, p	260 w			304 w, p	350 w, p
	$4ZnCl_2 \cdot 1KCl$	80 w, d	106 w, d	230 m, p	260 vw			304 w, p	340 w
	$3ZnCl_2 \cdot 1KCl$	80 w, d	106 w, d	230 m, p				304 m, p	350 w
	$2ZnCl_2 \cdot 1KCl$		95 w, d	235 w, d			290 s, p	304 w	
	$1ZnCl_2 \cdot 1KCl$	80 w, d	95 w, d	230 vw			290 s, p	310 vw	350 vw
	$1ZnCl_2 \cdot 3KCl$			230 vvw		270 s, p			360 vvw
	assignt			poly	Zn–Cl–Zn [b]	$ZnCl_4^{2-}$	$ZnCl_3^-$	$ZnCl_2$	$ZnCl^+$
9	$1ZnCl_2 \cdot 1KCl$	75 d		230 p			295 s, p		
	$5ZnCl_2 \cdot 6KCl$	75 d		230 p			291 s, p		
	$3ZnCl_2 \cdot 4KCl$	75 d					290 s, p		
	$2ZnCl_2 \cdot 3KCl$	75 d					286 s, p		
	$1ZnCl_2 \cdot 2KCl$		110 d			280 s, p			
	assignt					$ZnCl_4^{2-}$	poly [c]		

[a] Abbreviations: s, strong; m, medium; w, weak; vw, very weak; vvw, very very weak; p, polarized; d, depolarized; b, bridge Zn–Cl stretch; def, deformation; t, terminal Zn–Cl stretch; poly, $(ZnCl_2)_n$ polymer. [b] The band is assumed to be associated with an unstable species containing at least one Zn–Zl–Zn stretch. [c] These bands are assigned to a smaller $(ZnCl_2)_m$ polymer.

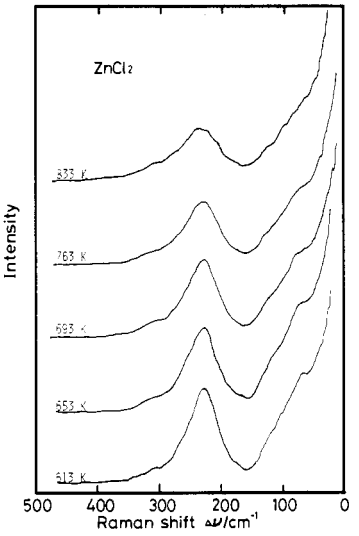

Figure 3. Temperature dependences of the Raman spectra of molten $ZnCl_2$.

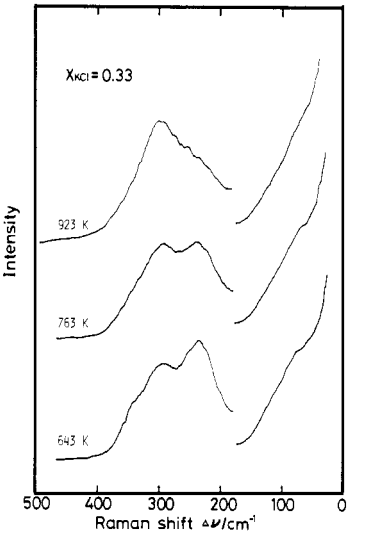

Figure 4. Temperature dependences of Raman spectra of the molten $ZnCl_2$–KCl system ($X = 0.33$). The sensitivity was changed above 175 cm^{-1} to observe the entire spectra clearly.

80 to 120 cm^{-1}. As pointed out by Bues and Brockner,[9] the latter band may be assigned to the deformation mode of Cl–Zn–Cl. However, we shall discuss no further details for this deformation mode because of the ill-defined band profiles. The two highly polarized Raman bands (ρ values of 0.02–0.05) in the range from 200 to 300 cm^{-1} corresponded to two different stretching vibrations with totally symmetric characters. The peak at 280 cm^{-1} in Figures 1 and 2 in the concentration range $1 > X \geq 0.67$ is assigned to the stretching mode of vibration from the isolated tetrahedral $ZnCl_4^{2-}$ ion, because no appreciable variation in the profile of the spectrum can be detected in the range $1 > X \geq 0.67$ and, moreover, the thermodynamic interaction parameter[13] obtained from EMF measurements by the present author shows a notable minimum at $X = 0.67$ where the population ratio Cl^-/Zn^{2+} is equal to 4. A slight peak shift from 280 cm^{-1} for $X = 0.67$ to 278 cm^{-1} for $X = 0.83$ suggests a change in the force constant of the A_1 mode

(13) Some of the authors (M.T. and T.N.) have investigated the enthalpy and entropy of mixing, ΔH^M and ΔS^M, in the molten $ZnCl_2$–KCl system by means of the EMF method. The interaction parameter $\Delta H^M/X(1 - X)$ showed a notable minimum at $X = 0.67$. The entropy of mixing showed a minimum around $X = 0.40$.

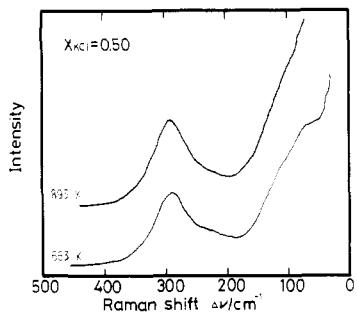

Figure 5. Temperature dependences of Raman spectra of the molten $ZnCl_2$–KCl system (X = 0.50).

in $ZnCl_4^{2-}$ with the increasing concentrations of K^+ ion surrounding the complex $ZnCl_4^{2-}$ ion. Figures 3–5 show the variation of Raman spectra with the increasing temperature where all the other experimental conditions are kept constant for each concentration. As shown in Figure 3, the 230-cm^{-1} band is always accompanied by a shoulder. This complicated band has been graphically separated by other workers[10,11,14] into three or four bands as shown in Table I. Angell and Wong[15] have investigated the structure of glassy and molten $ZnCl_2$ by means of far-IR, together with a Raman study. They assigned the 230-cm^{-1} band to the vibrational modes resulting from a network structure of $(ZnCl_2)_n$ polymer. The 230-cm^{-1} band decreases with increasing temperature, as shown in Figure 3, while the shoulder remains unchanged in magnitude. This result indicates that $(ZnCl_2)_n$ polymer dissociated partially into Raman-inactive fragment ions such as Zn^{2+}···Cl^-–Zn^{2+}, Zn^{2+}, ..., although the $(ZnCl_2)_n$ polymer remains as the main species. The increase in specific conductivity[16] with increasing temperature supports the partial dissociation. In contrast with our opinion, Yokō et al.[6] have reported that $(ZnCl_2)_n$ polymer does not exist above 727 K. Small humps on the profile of the 230-cm^{-1} band at the highest temperature (833 K) in Figure 3 suggest an existence of the other type of thermal dissociation.

A marked change in intensities of the 230- and 292-cm^{-1} bands for X = 0.33 shown in Figure 4 was observed as the temperature increased. However, as the spectrum between the two peaks showed a considerably complicated profile, these spectra will not be separated into only 230- and 290–292-cm^{-1} bands as reported previously.[10,11] We observed a minimum of entropy of mixing[13] around this concentration. These peculiar results suggest an existence of a complicated structure associated with the 292-cm^{-1} band. As shown in Figure 5, the spectra for X = 0.50 showed no remarkable change in the profiles and the peak height around 292 cm^{-1} except for a small decrease in height around 230 cm^{-1}.

The thermal excitation of $(ZnCl_2)_n$ polymer synchronized with the formation of the fragments may be treated by the following model of two bonding states,[15] >Zn–Cl– and >Zn···Cl–. We assume that the intensity I of the 230-cm^{-1} band is proportional to the number N_1 of bonding zinc–chlorine bonds, >Zn–Cl–, and that the thermal excitation can be measured by the number N_2 of dangling zinc–chlorine bonds, >Zn···Cl–. According to the method developed by Angell and Wong,[15] N_1 and N_2 satisfy the equation

$$N_2/N_1 = e^{-[\Delta H - T(\Delta S)]/RT} \quad (1)$$

where ΔH and ΔS are the changes in energy and vibrational entropy, respectively, associated with excitation of a zinc–chlorine bond. If we remember that $N_1 + N_2 = N_0$ is a constant, it follows from eq 1 that

$$N_1 = N_0/(1 + e^{-[\Delta H - T(\Delta S)]/RT}) \quad (2)$$

and

$$N_2 = N_0/(1 + e^{[\Delta H - T(\Delta S)]/RT}) \quad (3)$$

From eq 2 the Raman intensity for the 230-cm^{-1} band is given by

$$I = kN_1 = kN_0/(1 + e^{-[\Delta H - T(\Delta S)]/RT}) \quad (4)$$

or

$$\ln I = \ln (kN_1) = \ln (kN_0) - \ln (1 + e^{-[\Delta H - T(\Delta S))]RT}) = k' - \ln (1 + e^{-[\Delta H - T(\Delta S)]/RT}) \quad (5)$$

With the parameters of the excited states obtained by Angell and Wong[15]

$$\Delta H = 17.7 \text{ kJ/mol} \qquad \Delta S = 24.5 \text{ J/(mol deg)}$$

put into eq 5, ln I values were calculated and plotted vs. $1/T$ in Figure 6. In this study, the Raman intensity I was determined from a peak area in the wavenumber side lower than 230 cm^{-1}. The observed values of ln I agree well with the calculated curve in Figure 6 except for the values at 833 K. This result supports the two-state model.

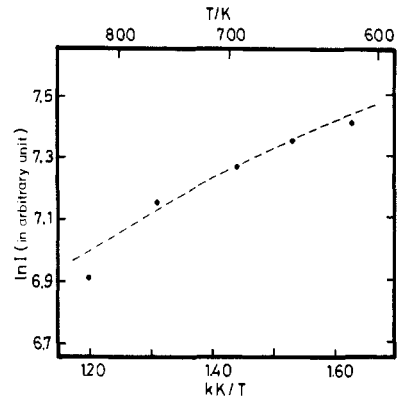

Figure 6. Plot of ln I vs. $1/T$. The dashed line shows the result calculated from eq 5 with parameters given by Angell and Wong.[15]

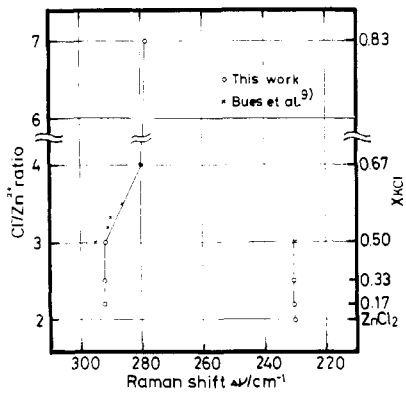

Figure 7. Relation of two totally symmetric peaks vs. the Cl^-/Zn^{2+} ratio.

In Figure 7 the locations of the two totally symmetric Raman peaks shown in Figure 1 are plotted against the Cl^-/Zn^{2+} ratio for the molten $ZnCl_2$–KCl system. Both peaks do not shift until the ratio Cl^-/Zn^{2+} reaches 3 (X = 0.50). In reference to the data by Bues and Brockner,[9] the peak on the lower wavenumber side disappears at the Cl^-/Zn^{2+} ratio of 3 (X = 0.50), and at this ratio the peak at the higher side (292 cm^{-1}) begins to shift linearly toward 280 cm^{-1}, where the

(14) Irish, D. E.; Young, T. F. *J. Chem. Phys.* **1965**, *43*, 1765.
(15) Angell, C. A.; Wong, J. *J. Chem. Phys.* **1970**, *53*, 1053.
(16) Easteal, A. J.; Angell, C. A. *J. Phys. Chem.* **1970**, *74*, 3987.

Cl^-/Zn^{2+} ratio equals 4 ($X = 0.67$). The appearance and behavior of the 292-cm^{-1} peak in Figure 7 indicate the presence of a certain kind of oscillator that is different from the above-mentioned $(ZnCl_2)_n$ polymer or the isolated $ZnCl_4^{2-}$ complex ion. It is surprising that this unknown oscillator has an appreciable thermal stability as is indicated by Figure 5.

Acknowledgment. The authors wish to express their sincere thanks to Professor Shirō Maeda and Mr. Shunsuke Kobinata, Research Laboratory of Resources Utilization, Tokyo Institute of Technology, for their kind instructions and permission to use their laser-Raman spectrophotometer. We also thank Dr. Noriko Itoh of our laboratory for her helpful discussions.

Registry No. $ZnCl_2$, 7646-85-7; KCl, 7447-40-7.

Contribution from the Department of Chemistry, University of Washington, Seattle, Washington 98195

Peroxo-Metal Bonding in $M(PH_3)_4(O_2)^+$, M = Co, Rh, Ir

Joe G. Norman, Jr.,* and P. Barry Ryan

Received January 20, 1982

Previously we presented a comparison of the electronic structures of $Pt(PH_3)_2(O_2)$ and $Pt(PH_3)_2(C_2H_4)$—theoretical models for archetypal group 8 peroxo and d^{10} ethylene complexes with PPh_3 ligands—based on SCF–Xα–SW calculations.[1] Though extremely well characterized, $Pt(PPh_3)_2(O_2)$ is somewhat special in that most group 8 peroxo complexes contain Co(III), Rh(III), or Ir(III)—i.e., d^6 rather than d^8 metals.[2] Typical are six complexes $M(PR_3)_4(O_2)^+$ with general structure depicted by I.[3] We undertook SCF–Xα–SW

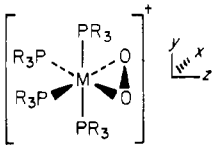

I

calculations on $M(PH_3)_4(O_2)^+$ and $M(PH_3)_4^{3+}$, M = Co, Rh, Ir, using averaged dimensions from these structures,[4] in order to help answer the following questions: (1) Why do the observed rate of formation from $M(PR_3)_4^+ + O_2$ and the final stability of the peroxo complexes vary in the order Co ≫ Ir > Rh?[5] Coordination of O_2 is reversible for Rh but essentially irreversible for Co and Ir. (2) How do the frontier orbitals, and d vs. s vs. p character of the metal's contribution to bonding, change down the column and compare to Pt-$(PH_3)_2(O_2)$? (3) What orbital transitions account for the observed electronic spectrum?[6,7]

Results and Discussion

Figure 1 compares the calculated frontier orbitals of the d^6 complexes with those of $Pt(PH_3)_2(O_2)$. These orbitals are

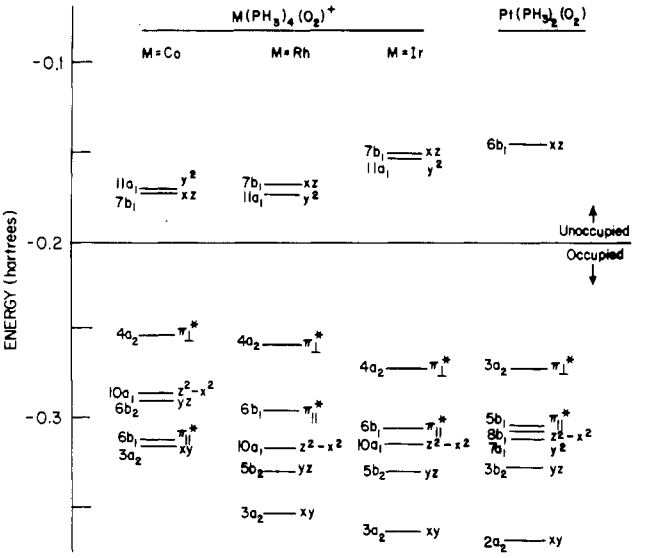

Figure 1. Highest occupied and lowest unoccupied SCF energy levels of $M(PH_3)_4(O_2)^+$, M = Co, Rh, Ir, and $Pt(PH_3)_2(O_2)$. Mainly metal d orbitals are designated by their subscripts (xy, yz, $z^2 - x^2$, xz, y^2) and mainly peroxide orbitals as either in the MP_2O_2 plane ($\pi^*_{\parallel}$) or perpendicular to it ($\pi^*_{\perp}$). There is one $M(PH_3)_4(O_2)^+$ orbital above −0.35 hartree, mainly M–P_{axial} bonding, which is not shown here. For M = Co it is $5b_2$ and is at −0.33 hartree. For M = Rh and Ir it is $6b_2$ and is at −0.31 hartree.

mainly either metal d or peroxo π^*.[8] The Pt and Ir complexes are very similar; they differ significantly only in the expected energy elevation of the d_{y^2}-like orbital in the latter due to addition of two y-axis PH_3 ligands and in the associated removal of two d-like electrons. When the d^6 complexes are viewed as perturbed octahedra, each has a filled triad of "t_{2g}" d-like orbitals (xy, yz, and $z^2 - x^2$) at low energy and an empty pair of "e_g" orbitals (xz, y^2) at high energy. For Rh and Ir, the two peroxo π^* orbitals lie between the two groups of d-like orbitals and are the HOMO's of the complex. The Co complex is unique in having two "t_{2g}" orbitals between the $\pi^*_{\parallel}$ and $\pi^*_{\perp}$ pair. This is mainly due to the decreasing ligand field splitting of the d-like orbitals as one moves up the column. One may calculate an effective Δ_0 as the difference in average "t_{2g}" and "e_g" orbital energies. The result is 2.74, 3.58, and 4.01 μm^{-1} for the Co, Rh, and Ir complexes, respectively.

Increasing ligand field splitting is often associated with increasing metal–ligand bond strength. However, here the total calculated bond energies[9] are found to follow the experimentally observed order of stability, i.e., Co ≫ Ir > Rh. This same trend is seen at the orbital level in the relative energies of the main M–O_2 bonding orbital, $6b_1$ (see Figure 1). The point is that Δ_0 reflects only the metal d component of the total bonding, while for these d^6 metals only one empty d orbital (xz) is available to accept electrons from the O_2^{2-} and two PH_3 ligands in the plane. Hence, the in-plane M–P and M–O bond strengths will be critically dependent on how effectively the metal can use its s, p_x, and p_z orbitals and hybridize them with d_{xz} for good overlap with the ligand orbitals.

(1) Norman, J. G., Jr. *Inorg. Chem.* **1977**, *16*, 1328.
(2) Vaska, L. *Acc. Chem. Res.* **1976**, *9*, 175.
(3) (a) Terry, N. W.; Amma, E. L.; Vaska, L. *J. Am. Chem. Soc.* **1972**, *94*, 653. (b) McGinnety, J. A.; Payne, N. C.; Ibers, J. A. *Ibid.* **1969**, *91*, 6301. (c) Nolte, M. J.; Singleton, E.; Laing, M. *Ibid.* **1975**, *97*, 6396; *J. Chem. Soc., Chem. Commun.* **1975**, 660; *Acta Crystallogr., Sect. B* **1975**, *B31*, 2223; **1976**, *B32*, 1412, 1838.
(4) Sphere radii, α values, basis functions, etc. were chosen as in our previous calculations.[1] Note that the coordinate system used here has the C_2 axis along z rather than along x as in ref 1; this interchanges b_1 and b_2 orbitals. A Fenske–Hall calculation on $Co(PH_3)_4(O_2)^+$ is described in: Teo, B. K.; Li, W.-K. *Inorg. Chem.* **1976**, *15*, 2005.
(5) Vaska, L.; Chen, L. S.; Miller, W. V. *J. Am. Chem. Soc.* **1971**, *93*, 6671.
(6) Miskowski, V. M.; Robbins, J. L.; Hammond, G. S.; Gray, H. B. *J. Am. Chem. Soc.* **1976**, *98*, 2477.
(7) Lever, A. B. P.; Gray, H. B. *Acc. Chem. Res.* **1978**, *11*, 348.
(8) The occupied and unoccupied d-like orbitals are 54–89% and 41–52% metal, respectively; their metal character is 92–100% d. The peroxo π^*-like orbitals are 4–14% metal.
(9) Relative bond energies were obtained by subtracting from the calculated total energies the metal hyper-Hartree–Fock atomic energies[10] on which the choice of α values for the MO calculations is based. If the Rh-complex value thus obtained is taken as the zero point, the results for the complexes are −518, 0, and −40 kJ/mol for M = Co, Rh, and Ir, respectively. While Xα–SW total energies are well-known to be limited in accuracy, relative values for complexes as closely related as these should be meaningful.
(10) Mann, J. B. *Los Alamos Sci. Lab.*, [*Rep.*] *LA* **1967**, *LA-3690*.

0020-1669/82/1321-3555$01.25/0